Evidence of strong radiation reaction in the field of an ultra-intense laser

K. Poder,[1] M. Tamburini,[2] G. Sarri,[3, 4] A. Di Piazza,[2] S. Kuschel,[5, 6]

C. D. Baird,[7] K. Behm,[8] S. Bohlen,[9] J. M. Cole,[1] D. J. Corvan,[3] M. Duff,[10]

E. Gerstmayr,[1] C. H. Keitel,[2] K. Krushelnick,[8] S. P. D. Mangles,[1]

P. McKenna,[10] C. D. Murphy,[7] Z. Najmudin,[1] C. P. Ridgers,[7] G. M. Samarin,[3]

D. Symes,[11] A. G. R. Thomas,[8, 12] J. Warwick,[3] and M. Zepf[3, 5, 6]

[1]*The John Adams Institute for Accelerator Science,*
Blackett Laboratory, Imperial College London, London SW7 2AZ, UK

[2]*Max-Planck-Institut für Kernphysik,*
Saupfercheckweg 1, D-69117 Heidelberg, Germany

[3]*School of Mathematics and Physics, Queen's University Belfast,*
University Road, Belfast BT7 1NN, UK

[4]*corresponding author*

[5]*Helmholtz Institute Jena, Fröbelstieg 3, 07743 Jena, Germany*

[6]*Institut für Optik und Quantenelektronik,*
Friedrich-Schiller-Universität Jena, Max-Wien-Platz 1, 07743 Jena, Germany

[7]*Department of Physics, University of York,*
Heslington, York, YO10 5DD, United Kingdom

[8]*Center for Ultrafast Optical Science, University of Michigan,*
Ann Arbor, Michigan 481099-2099, USA

[9]*Deutsches Elektronen Synchrotron DESY, Hamburg 22607, Germany*

[10]*Department of Physics, SUPA, University of Strathclyde, Glasgow, G4 0NG, UK*

[11]*Central Laser Facility, Rutherford Appleton Laboratory,*
Didcot, Oxfordshire OX11 0QX, UK

[12]*Lancaster University, Lancaster LA1 4YB, United Kingdom*

(Dated: January 10, 2018)

Abstract

The description of the dynamics of an electron in an external electromagnetic field of arbitrary intensity is one of the most fundamental outstanding problems in electrodynamics. Remarkably, to date there is no unanimously accepted theoretical solution for ultra-high intensities and little or no experimental data. The basic challenge is the inclusion of the self-interaction of the electron with the field emitted by the electron itself – the so-called radiation reaction force. We report here on the first experimental evidence of strong radiation reaction, in an all-optical experiment, during the propagation of highly relativistic electrons through the field of an ultra-intense laser. In their own rest frame, the highest energy electrons experience an electric field as high as one quarter of the critical field of quantum electrodynamics and, accordingly, the experimental data gives a first indication of emerging of quantum effects in the electron dynamics. These results pave the way for the systematic study of strong radiation reaction in compact laser laboratories, an essential step towards the understanding of strong-field quantum electrodynamics.

In the realm of classical electrodynamics, the problem of radiation reaction (RR) is satisfactorily described by the Landau-Lifshitz (LL) equation [1], which has been theoretically demonstrated to be the self-consistent classical equation of motion for a charged particle [1, 2]. However, when the electron experiences extremely intense fields the LL equation may no longer be assumed valid [3]. A full quantum description is thus required and this is currently the subject of active theoretical research (see, for instance, Refs. [3–10]). Purely quantum effects can be triggered in these conditions, including the stochastic nature of photon emission [5, 6], a hard cut-off in the maximum energy of the emitted photons [9], and pair production [10].

Besides the intrinsic fundamental interest in investigating this regime in laboratory experiments, RR is often invoked to explain the radiative properties of powerful astrophysical objects, such as pulsars and quasars [11, 12]. A detailed characterisation of RR is also important for a correct description of high-field experiments using the next generation of multi-petawatt laser facilities, such as the Extreme Light Infrastructure [13], Apollon [14], Vulcan 20PW [15], and XCELS [16] where focussed intensities exceeding 10^{23} W/cm^2 are expected. The data presented here paves the way for detailed experimental studies of RR and high-field quantum electrodynamics in a laser-driven configuration.

The LL equation is obtained assuming that the electromagnetic field in the rest frame of the electron is much smaller than the classical critical field $F_0 = 4\pi\epsilon_0 m_e^2 c^4/e^3 \approx 1.8 \times 10^{20}$ V/m [1] and constant over distances of the order of the classical electron radius $r_0 = e^2/4\pi\epsilon_0 m_e c^2 \approx 2.8 \times 10^{-15}$ m. These conditions are automatically satisfied in classical electrodynamics since quantum effects are negligible as long as the rest frame fields are much smaller than the critical field of Quantum Electrodynamics (QED) $F_{cr} = \alpha F_0 \approx 1.3 \times 10^{18}$ V/m $\ll F_0$ [9] and remain constant over distances of the order of the reduced Compton wavelength $\lambda_C = r_0/\alpha \approx 3.9 \times 10^{-13}$ m $\gg r_0$ ($\alpha \approx 1/137$ is the fine structure constant). An electric field with amplitude of the order of the critical field F_{cr} is able to impart an energy of the order of mc^2 to an electron over a length of the order of λ_C. If the amplitude of the laser field in the rest frame of the electron is of the order of F_{cr}, the quantum recoil undergone by the electron when it emits a photon is thus not negligible [10]. Also, if the laser wavelength in the rest frame of the electron is of the order of λ_C, then already the absorption of a single laser photon would impart to the electron a recoil comparable with its rest energy. Even for GeV electrons with Lorentz factor $\gamma_e \gtrsim 2000$, the

micron-scale wavelength of typical high-power laser systems ($\lambda_L \approx 0.8 - 1\mu$m) implies that the only relevant condition on classicality is on the laser field amplitude F_L, which can be expressed by stating that the quantum parameter $\chi \approx (1 - \cos\theta)\gamma_e F_L/F_{cr}$ has to be much smaller than unity. Here θ is the angle between the laser propagation direction and the electron momentum in the laboratory frame. Thus the validity of the LL approach can be expected to break down when quantum effects on the electron's motion become important, i.e., when χ becomes a sizeable fraction of unity. In the intense fields that can be created by modern-day lasers, one must also account for the possibility of multiple laser-photons being absorbed and resulting in the emission of a single high-energy photon by the electron. For each photon formation length the number of absorbed photons per electron is of the order of the laser dimensionless amplitude $a_0 = eF_L\lambda_L/2\pi m_e c^2$ [10]. Available lasers can now easily reach $a_0 \gg 1$, thus allowing for experimental investigations of this strong-field regime.

The multi-GeV electrons available at accelerator laboratories world-wide would provide an excellent basis for RR studies in the non-linear and quantum regime, but are rarely available concurrently with ultra-intense lasers. The development of compact laser-driven wakefield accelerators (LWFA) [17] provides a well-suited alternative, since it allows GeV electron beams to be generated directly at high power laser laboratories capable of achieving field strengths of $a_0 \gg 1$. The plausibility of such an experimental approach is evidenced by the observation of non-linearities in Compton scattering in previous experimental campaigns [18–20], motivating the study reported here.

To date, only one laser-based experimental campaign has reached a non-negligible value of $\chi \approx 0.2$ [21, 22]. Whilst these experiments gave evidence of non-linearities in Compton scattering ($a_0 < 1$) [21] and generation of electron-positron pairs [22], no measurements were performed to directly assess the level of RR in the spectrum of the scattered electron beam. Moreover, despite the high field achieved in the electron rest frame, the relatively low intensity of the scattering laser ($a_0 \approx 0.3 - 0.4$) implies that single photon absorption was the dominant absorption mechanism in the electron dynamics in the field. Non-linearities only occurred perturbatively; the relative strength of the emission of the nth harmonic scales as a_0^{2n}, implying that non-linear Compton scattering was strongly suppressed. In our experimental configuration, a much higher laser intensity ($a_0 \simeq 10$) allowed a strongly non-linear regime of RR to be accessed for the first time (i.e., multi-photon absorption even within a single photon formation length). Thanks to the simultaneous high intensity and non-

negligible quantum parameter, the study reported in this manuscript thus represents the first experimental achievement in an all-optical setup of a strong-field quantum electrodynamic regime.

In this experiment we obtained a maximum quantum parameter $\chi \approx 0.25$ by interacting a multi-GeV electron beam (maximum Lorentz factor $\gamma_e \approx 4 \times 10^3$) [23] with a high intensity laser pulse ($\lambda_L = 0.8\ \mu$m and $a_0 \approx 10$). Under these circumstances the energy loss due to RR becomes substantial (up to 30% for the highest energy electrons in our simulations) and requires RR to be included in any model of the electron dynamics. Indeed, a perturbative model based on the power emitted according to the Larmor formula - and thus neglecting radiation reaction effects - is seen to greatly overestimate the observed energy loss in the electron beam. To the best of our knowledge, this is the first direct experimental evidence of strong radiation reaction of an electron in an ultra-intense laser field.

The experimental set-up is shown schematically in Fig. 1a. One of the twin laser beams of the Astra Gemini laser system (Driver Laser in Fig. 1a), was focussed at the entrance of a helium-filled gas-cell producing an electron beam via LWFA with an energy spectrum extending to approximately 2 GeV. The electron source size (FWHM diameter) is estimated to be $D_e \leq 1\ \mu$m and the energy dependent beam divergence was measured to be in the range of 0.7 mrad for electrons exceeding 1 GeV (see Methods for further details).

The second laser beam (Scattering Laser in Fig. 1a) was focussed, in a counter-propagating geometry, 1 cm downstream from the end of the gas-cell, with a measured intensity distribution as shown in Fig. 1b. At this point the GeV electron beam had expanded to a diameter of approximately 8 μm. Due to the inherent lag of the laser-accelerated electron beam in respect to the driver laser, the scattering laser has defocussed for approximately 64 fs before interacting with the electrons (see Methods for details). Numerical calculations indicate that, at this time, the laser has defocussed to a rather flat intensity distribution with a peak dimensionless amplitude of $a_0 \simeq 10$ and a full width half maximum of 7 μm (see Fig. 1c). After the interaction with the laser field, the electrons were spectrally resolved by a magnetic spectrometer whereas the energy contained in the Compton-generated γ-ray beam was measured using a caesium-iodide (CsI) scintillator. Further details on the experimental configuration are given in the Methods section.

The LWFA generating GeV level electron beams [23, 24] was run in a regime where the spectral shape of the electron beam was a stable and reproducible function of the input

laser energy (Fig. 2). In Fig. 2.a, we show the correlation between the energy of the laser driving the wakefield and the cut-off energy of the accelerated electron beam (see Methods for details). The empty squares depict shots with the scattering laser off with the dashed line showing a linear fit. The vast majority of these shots fall within 1σ (68% confidence) with all of them still within a 2σ band (95% confidence). The colour-coded circles depict shots with the scattering laser on. The colour of each circle represents the total energy of the photon beam emitted via Compton scattering, as recorded by the CsI scintillator. The energies of both the driver and scattering laser were measured live on each shot, allowing to clearly identify suitable reference shots (scattering laser off) for each shot with the scattering laser on.

The intrinsic shot-to-shot pointing fluctuations of LWFA beams [25] results in a statistical fluctuation of the spatial overlap of the laser spot with the electron beam. To discern between shots of poor and good overlap we use the energy contained in the Compton γ-ray beam generated during the interaction, an established method for this class of experiments (see, for instance, Ref. [21]). To record this, a 5 cm thick caesium-iodide (CsI) scintillator was placed 4 m downstream of the interaction. Further details on the CsI detector are given in the Methods section. The total energy emitted via Compton scattering scales as $E_{ph} \propto \int a_0 \gamma_e^2 N_e(a_0) \, da_0$, with $N_e(a_0)$ the number of electrons interacting with a field of amplitude a_0 [26]. Whilst our CsI detector did not allow us to extract the spectral distribution of the photon beam, the signal recorded still allows us to discern between shots with best overlap (and, therefore, both higher energy loss in the electron beam and photon yield) from those with poorer overlap. This is exemplified in Fig. 2a. Shots with relatively low photon yield mostly fall within the 2σ band of the linear dependence of the electron beam cut-off energy on the energy of the driver laser. On the other hand, the two shots with the brightest photon signal (labelled with $\underline{d}$ and $\underline{c}$ in Fig. 2a) both fall outside the 2σ band, implying that the probability of them being just the result of a random fluctuation is smaller than 0.2%. This places high confidence that a measurement of a lower electron energy is directly related to the occurrence of strong RR.

We will therefore focus our attention only on shots where the CsI detector indicates best overlap between the high-energy component of the electron beam and the scattering laser (shots $\underline{c}$ and $\underline{d}$ in Fig. 3a). A comparison between the measured spectral energy density of the initial (scattering laser off) and scattered (scattering laser on) electron beam for conditions

of best overlap is shown in Fig. 3d. The corresponding single-shot spectral energy densities and the associated uncertainties for the reference electron beams are shown in Fig. 2d and exhibit a spectral profile that decreases with energy up to 2 GeV, with a clear peak at approximately 1.2 GeV. The spectral energy density of the electrons after the interaction with the scattering laser beam (red line in Fig. 3d) not only shows a reduction in the cut-off energy but also a significant change in spectral shape, with virtually no electrons with energy exceeding 1.6 GeV. Moreover, the local maximum in the spectrum is now shifted down to an energy of approximately 1 GeV and there is clear accumulation of electrons at lower energies, suggesting a net energy loss for the highest energy electrons of the order of 30%.

The overall electron energy loss is slightly lower than a classical estimate based on the LL equation. For our experiment, we can assume a plane wave with a Gaussian temporal field profile given by $\exp(-\varphi^2/\sigma_\varphi^2)$, where $\varphi = \omega_L(t - z/c)$ is the laser phase, ω_L is the laser angular frequency, and $\sigma_\varphi = \omega_L t_L/\sqrt{2\log 2}$. Here t_L represents the FWHM of the laser intensity. In this case, the analytical solution of the LL equation [27], provides:

$$\frac{\Delta\gamma_e}{\gamma_e} \approx \frac{\sqrt{\pi/\log 2}\,\tau_0 t_L \omega_L^2 \gamma_e a_0^2/2}{1 + \sqrt{\pi/\log 2}\,\tau_0 t_L \omega_L^2 \gamma_e a_0^2/2}, \tag{1}$$

with $\tau_0 = 2r_0/3c \approx 6.3 \times 10^{-24}$ s, $t_L = 42 \pm 3$ fs the laser duration, and $\omega_L = 2.4 \times 10^{15}$ rad/s the laser carrier frequency (see also Ref. [28], where there t_L corresponds to σ_φ/ω_L in our notation). For $\gamma_e = 4000$ and $a_0 = 10$, the LL equation predicts an energy loss of about 40%, slightly higher than the experimental findings. We observe that under the present experimental conditions (ultrarelativistic electrons with $\gamma_e \gg a_0$ and initially counterpropagating with respect to the laser field) it is possible to approximate $\gamma_e \approx \gamma_e(1 - v_{e,z}/c)/2$, with $v_{e,z} \approx -c$ being the electron velocity along the propagation direction of the laser field, and thus use directly Eqs. (8) and (9) in [27] to estimate the relative energy loss.

A quantitative comparison between the experimental data and the theoretical models requires a detailed comparison of the measured spectra with those predicted by different models using the reference spectra as input. Fig. 4 shows the normalised experimental spectral energy density of the scattered electrons in conditions of best overlap and the corresponding theoretical curves obtained by simulating the effect of the scattering laser on reference spectra using different models and both a multi-particle code and a Particle-In-Cell

(PIC) code. Both multi-particle and PIC approaches are described in detail in the Methods section. The error bands of the multi-particle code correspond to the uncertainties in the reference electron spectra as well as uncertainties in the intensity of the scattering laser (see Methods).

The models implemented within the multi-particle approach correspond to different degrees of approximation. The green band in Fig. 4a depicts the results of a model routinely used in synchrotrons [29]. In this case, the electron trajectory is calculated via the Lorentz force and the electron energy loss is only accounted for by subtracting the total energy emitted by each electron after the laser-electron interaction. In this regime, RR is thus neglected during the passage of the electron through the laser field. This approach fails to describe the data, greatly overestimating the energy loss and thus providing a strong indication that a proper treatment of RR is required to correctly model the dynamics of the electrons. Fig. 4b depicts the results from the LL equation, which is able to reproduce the characteristic spectral shape of the scattered electrons and exhibits a much closer agreement with the experimental data overall. Despite the rather large uncertainty in the data, it is interesting to note that there is a first preliminary indication of the LL equation slightly overestimating the energy loss experienced by the electron beam. Even though the experimental data does not allow us to draw a definite conclusion in this regard, a slight overestimate of the energy loss is to be expected due to the non-negligible value of the quantum parameter χ in this experiment since, strictly speaking, the LL is valid only under the assumption of $\chi \ll 1$. This overestimate is due to the fact that the LL equation does not include the hard cut-off in the maximum energy of the emitted photons predicted by quantum physics (see, for instance, Ref. [10]) and, therefore, overestimates the total energy of the emitted photons.

The effect of the hard quantum cut-off can be phenomenologically included in the model by multiplying the radiation reaction force in the LL equation by a "weighting" function $g(\chi) = I_Q/I_C$ [30], where I_Q and I_C are the quantum and classical intensities of the emitted radiation, respectively (see Methods). In this way, the known classical overestimate of the total emitted energy with respect to the more accurate quantum expression is avoided. However, in this "semi-classical" model the emission of radiation is still included as a "classical" continuous process, i.e., the quantum stochastic nature of photon emission is ignored. Moreover, we point out that the used expression of I_Q is derived within the so-called local-constant-crossed field approximation. This approximation is described in more detail below,

where the results according to the full quantum model are reported. A comparison between the predictions of this model and the experimental results is shown in Fig. 4c. The improved agreement of the semi-classical LL model compared to the unmodified LL provides a preliminary indication of the onset of quantum effects under the conditions of the experiment.

Finally, a comparison between the experimentally measured spectrum of the scattered electrons and numerical calculations based on a multi-particle QED code (green curve) is shown in Fig. 4d. This model is, within the uncertainties of the experiment, able to reproduce the general features of the experimental data. However, there still is a non-negligible mismatch, especially in the shape of the spectral energy density. In order to rule out collective effects in the electron beam, matching 3-dimensional PIC simulations using the code EPOCH [31] have also been carried out (see Methods). Indeed, the PIC and the multi-particle QED model yield very similar results showing that collective effects are negligible in our experimental conditions (see Fig. 4.d). In addition, we stress that we have performed an extensive parametric scan on the laser amplitude and on the position of the interaction point without being able, in particular, to reproduce the experimental spectral shape with the quantum model. One possible source of mismatch arises from the fact that the so-called local-constant-crossed field approximation [10], a common approximation adopted in this class of calculations that assumes $a_0 \gg 1$, may not be accurate at the moderate a_0 achieved in the experiment. In this respect, this might be a first hint on the failure of this approximation in our experimental regime [32]. This approximation requires that within the formation length of the emission process, typically of the order of λ_L/a_0 [10], the laser field changes slowly. In our case we obtain formation lengths of the order of tens of nm, which are not negligible if compared to the laser wavelength. Other possible reasons for the discrepancy include the experimental limitations regarding knowledge of quantities such as the phase content and longitudinal distribution of the laser beam. It is less evident why, despite the experimental uncertainties, the semi-classical model seems to reproduce slightly more accurately the shape of the experimental spectra than the quantum model. Both models, in fact, rely on the local-constant-crossed field approximation. Unlike the quantum model, though, the semi-classical model exploits this approximation only in the expression of I_Q, whereas the basic equation (the LL equation) is exact in a_0 although within the classical regime. In this respect, we can only conclude that in our experiment the stochasticity

9

effects, which are included in the quantum model but not in the semi-classical model, are less important than effects beyond the local-constant-crossed field approximation, which are at least partially still included in the semi-classical model, being based on the LL equation.

We have also performed a series of simulations, assuming a semi-classical model of RR, in order to check whether a weaker electron energy loss might be attributed to a slight transverse misalignment between the electron beam momenta and the direction of propagation of the scattering laser. This misalignment is expected to occur statistically on a shot-to-shot basis, due to random fluctuation in electron beam pointing. As an example, a shot with a weaker energy loss (labelled with c in Fig. 2.a) is well reproduced by the semi-classical calculations if an impact parameter of 5 μm is assumed (see Supplementary material).

In conclusion, we report on the first experimental detection of strong radiation reaction in an all-optical experiment. The experimental data give clear evidence of significant energy loss ($> 30\%$) of ultra-relativistic electrons during their interaction with an ultra-intense laser field. In their own rest frame, the highest energy electrons experience an electric field as high as one fourth of the critical field of QED. The experimental data can only be theoretically explained by taking into account radiation reaction occurring during the propagation of the electrons through the laser field, and best agreement is found for the semi-classical correction of the Landau-Lifshitz equation.

REFERENCES:

[1] L. D. Landau, and E. M. Lifshitz, <u>The classical theory of fields</u> (Butterworth-Einemann, Amsterdam, 2000, paragraph 76).

[2] V. S. Krivitskii, and V. N. Tsytovich, "Average radiation-reaction force in quantum electrodynamics", Sov. Phys. Usp. **34**, 250 (1991).

[3] A. Di Piazza <u>et al.</u>, "Extremely high-intensity laser interactions with fundamental quantum systems", Rev. Mod. Phys. **84**, 1177 (2012) and references therein.

[4] M. Chen, E. Esarey, C. G. R. Geddes, C. B. Schroeder, G. R. Plateau, S. S. Bulanov, S. Rykovanov, and W. P. Leemans, "Modeling classical and quantum radiation from laser-plasma accelerators", Phys. Rev. ST Accel. Beams **16**, 030701 (2013).

[5] N. Neitz, A. Di Piazza, "Stochasticity Effects in Quantum Radiation Reaction", Phys. Rev. Lett. **111**, 054802, (2013).

[6] T. G. Blackburn et al., "Quantum Radiation Reaction in Laser-Electron Beam Collisions", Phys. Rev. Lett. **112**, 015001 (2014).

[7] M. Vranic, T. Grismayer, R. A. Fonseca, and L. O. Silva, "Quantum radiation reaction in head-on laser-electron beam interaction", New J. Phys. **18**, 073035 (2016).

[8] V. Dinu, C. Harvey, A. Ilderton, M. Marklund, G. Torgrimsson, "Quantum Radiation Reaction: From Interference to Incoherence", Phys. Rev. Lett. **116**, 044801 (2016).

[9] V. B. Berestetskii, E. M. Lifshitz, and L. P. Pitaevskii, <u>Quantum Electrodynamics</u> (Elsevier Butterworth-Heinemann, Oxford, 1982).

[10] V. I. Ritus, "Quantum effects of the interaction of elementary particles with an intense electromagnetic field", J. Russ. Laser Res. **6**, 497 (1985).

[11] R. Ruffini, G. Vereshchagin, and S. Xue, "Electron-positron pairs in physics and astrophysics: From heavy nuclei to black holes", Phys. Rep. **487**, 1 (2010).

[12] J. Sultana, D. Kazanas, and A. Mastichiadis, "The supercritical pile gamma-ray burst model: The GRB afterglow steep-decline-and-plateau phase", Astrophys. J. **779**, 16 (2013).

[13] I. C. E. Turcu <u>et al.</u>, "High field physics and QED experiments at ELI-NP", Romanian Reports in Physics, **68** Supplement, S145 (2016).

[14] J. P. Zou et al., "High Power Laser Science and Engineering Design and current progress of the Apollon 10 PW project", High Power Laser Science and Engineering **3**, e2 (2015).

[15] http://spie.org/x103688.xml

[16] http://www.xcels.iapras.ru/2013_news.html

[17] E. Esarey, C. Schroeder, and W. Leemans, "Physics of laser-driven plasma-based electron accelerators", Rev. Mod. Phys. **81**, 1229 (2009) and references therein.

[18] G. Sarri et al., "Ultrahigh Brilliance Multi-MeV Gamma-Ray Beams from Nonlinear Relativistic Thomson Scattering", Phys. Rev. Lett. **113**, 224801 (2014).

[19] K. Khrennikov et al., "Tunable All-Optical Quasimonochromatic Thomson X-Ray Source in the Nonlinear Regime", Phys. Rev. Lett. **114**, 195003 (2015).

[20] W. Yan et al., "High-order multiphoton Thomson scattering", Nat. Phot. published online: doi:10.1038/nphoton.2017.100

[21] C. Bula et al., "Observation of Nonlinear Effects in Compton Scattering", Phys. Rev. Lett. **76**, 3116 (1996).

[22] D. L. Burke et al., "Positron Production in Multiphoton Light-by-Light Scattering", Phys. Rev. Lett. **79**, 1626 (1997).

[23] K. Poder et al., "Multi-GeV electron acceleration in wakefields strongly driven by oversized laser spots", in preparation

[24] S. Kneip et al., "Near-GeV Acceleration of Electrons by a Nonlinear Plasma Wave Driven by a Self-Guided Laser Pulse", Phys. Rev. Lett. **103**, 035002 (2009)

[25] G. M. Samarin, M. Zepf, and G. Sarri, "Radiation reaction studies in an all-optical set-up: experimental limitations" J. Mod. Opt. DOI: 10.1080/09500340.2017.1353655 (2017).

[26] S. Corde et al., "Femtosecond x rays from laser-plasma accelerators", Rev. Mod. Phys. **85**,1 (2013).

[27] A. Di Piazza, "Exact solution of the Landau-Lifshitz equation in a plane wave", Lett. Math. Phys. **83**, 305 (2008).

[28] A. G. R. Thomas, C. P. Ridgers, S. S. Bulanov, B. J. Griffin, and S. P. D. Mangles, "Strong Radiation-Damping Effects in a Gamma-Ray Source Generated by the Interaction of a High-Intensity Laser with a Wakefield-Accelerated Electron Beam", Phys. ReV. X **2**, 041004 (2012).

[29] G. Stupakov, and S. Heifets, "Beam instability and microbunching due to coherent synchrotron radiation", Phys. Rev. ST Accel. Beams **5**, 054402 (2002).

[30] J. G. Kirk, A. R. Bell, and I. Arka "Pair production in counter-propagating laser beams", Plasma Phys. Contr. F. **51**, 085008 (2009).

[31] T. D. Arber et al., "Contemporary particle-in-cell approach to laser-plasma modelling", Plasma Phys. Control. Fusion, **57**, 113001 (2015).

[32] A. Di Piazza, S. Meuren, M. Tamburini, and C. H. Keitel, "On the validity of the local constant field approximation in nonlinear Compton scattering", arXiv:1708.08276 (2017).

[33] S. Kneip et al., "Bright spatially coherent synchrotron X-rays from a table-top source", Nat. Phys. **6**, 980 (2010).

[34] D. J. Corvan et al., "Optical measurement of the temporal delay between two ultra-short and focussed laser pluses", Opt. Expr. **24**, 3127 (2016).

[35] C. Gregory, private communication.

[36] H. D. Zhang et al., "Beam halo imaging with a digital optical mask", Phys. Rev. ST-AB **15**, 072803 (2012).

[37] G. Battistoni et al., "The FLUKA code: description and benchmarking", AIP Conf. Proc. **896**, 31 (2007).

[38] M. Tamburini et al., "Radiation reaction effects on radiation pressure acceleration", New J. Phys. **12**, 123005 (2010).

[39] V. N. Baier, V. M. Katkov, V. M. Strakhovenko, *Electromagnetic Processes at High Energies in Oriented Single Crystals*, (World Scientific, Singapore, 1998).

[40] M. Tamburini, A. Di Piazza, C. H. Keitel, "Laser-pulse-shape control of seeded QED cascades", Sci. Rep. **7**, 5694 (2017). See also arXiv:1511.03987 (2015).

[41] C.P. Ridgers et al., "Modelling Gamma Ray Emission and Pair Production in High-Intensity Laser-Matter Interactions", J. Comp. Phys., **260**, 273 (2014).

[42] doi:10.15124/bd4a4a0b-78e3-405c-9318-1757b0209c54.

METHODS

Laser-wakefield accelerated electron beam: The electron beam was generated and accelerated during the propagation of an intense laser beam through a 2 cm long gas-cell filled with helium at a background pressure of 60 mbar that, once fully ionised, corresponds to an electron density of 2×10^{18} cm^{-3}. The laser with a pulse duration of (42 ± 3) fs was focussed using an $f/40$ spherical mirror down to a focal spot with Full-Width-Half-Maxima (FWHM), along the two axis, of $\sigma_x = (59 \pm 2)$ µm and $\sigma_y = (67 \pm 2)$ µm containing

9 J (normalised intensity of $a_0 \approx 1.7$). The laser beam accelerated electrons with a broad energy spectrum exceeding 2 GeV ($\gamma_e \approx 4 \times 10^3$). The cut-off energy of the LWFA-generated electron beam is seen to be linearly dependent on the energy of the driving laser, which is measured live on each shot by integrating the beam near-field on a camera that has been calibrated against an energy meter. The cut-off energy is defined as the energy at which the spectral intensity falls to 10% of the peak value. Our analysis is based on single-electron spectra normalised by dividing the measured spectrum by the overall number of electrons with energy exceeding 350 MeV, in order to eliminate shot-to-shot fluctuations in the total electron number without affecting the spectral shape of the beam. The electron beam source size can be estimated to be $D_e \leq 1\,\mu\text{m}$, as deduced by rescaling the size of typical betatron sources in similar conditions [33]. The energy-dependent beam divergence was determined by measuring the beam width perpendicular to the direction of dispersion on the electron spectrometer screen 2 m downstream from the gas cell. For electron energies exceeding 1 GeV, the divergence is measured to be $\theta_e = (0.70 \pm 0.05)$ mrad. Even though this gives in principle only the divergence along one of the transverse dimensions of the beam, the regime of laser-wakefield acceleration we are operating in should produce cylindrically symmetric beams. A suitable fit of the measured electron beam divergence θ_e with respect to the electron energy E_e gives:

$$\theta_e\,[\texttt{mrad}] = 30.44\exp(-10^{-2}E_e\,[\texttt{MeV}]) + 0.7, \tag{2}$$

where θ_e is the FWHM of a Gaussian distribution with mean zero.

This relation was used as an input for the numerical simulations used to model the experiment. Space charge effects are negligible for electron energies exceeding 100 MeV, justifying the assumption of the electron beam divergence being constant throughout the propagation to the detector.

The scattering laser: one of the two laser beams (pulse duration of (42 ± 3) fs, energy after compression of (8.8 ± 0.7) J) of the Astra-Gemini system was focused, using an $f/2$ off-axis parabola with a concentric $f/7$ hole (energy loss of 10%), 1 cm downstream of the exit of the gas-cell. The scattering and driver laser are linearly polarised along perpendicular axis (horizontal and vertical, respectively) in order to further reduce risks of back-propagation of

the lasers in the amplification chains. Both lasers are generated from the same oscillator and synchronised using a spectral interferometry technique discussed in Ref. [34] and already used in a similar experimental setup [18]. The system had a temporal resolution of approximately 40 fs. The radial distribution of the laser intensity at focus is shown in Fig. 1b. and it arises from an average of ten consecutive measurements at low power (spatial resolution of the detector of 0.2 µm/pixel). Independent measurements of the intensity profile at low-power and full-power indicate a broadening of the focal spot radius of the order of 10% in the latter case [35]. This effect is taken into account in the computed transverse laser field distribution shown in Fig. 1c.

The energy of both the Driver and Scattering laser have been measured, live on each shot, by integrating the beam near-field on a camera that was previously absolutely calibrated against an energy meter.

Due to the temporal lag between the driver laser and the accelerated electrons, we expect the scattering laser to have defocussed for approximately 64 fs before interacting with the electrons [17, 23]. At this time delay, the scattering laser has a rather flat profile, with a peak a_0 of the order of 10 and a full width half maximum of 7 µm. Measurements of the pointing fluctuation of the laser-driven electron beam indicate, as an average over 100 consecutive shots, an approximately Gaussian distribution (confidence of 95% from the Kolmogorov-Smirnov test) centred on the laser propagation axis with a standard deviation of (3.2 ± 0.8) mrad [25].

The magnetic spectrometer: the magnetic spectrometer consisted of a 15 cm long dipole magnet with a peak magnetic field of 1.0 T. The magnet was placed 60 cm from the laser-electron interaction point and the dispersed electron beam was recorded by a LANEX scintillator screen placed 2 m away from the gas-cell. The screen was tilted by 45°, to improve spectral resolution. The minimum electron energy recorded on the LANEX screen in this configuration was 350 MeV. The LANEX screen was imaged in a Scheimplflug configuration [36], allowing the whole length of the screen to be in focus even at the 45° viewing angle. Given a divergence of the highest energy electrons of $\theta_e \approx 0.7$ mrad, and a beam source size of $D_e \leq 1$ µm, the spectral resolution of the magnetic spectrometer can be estimated, for ultra-relativistic electrons, as:

$$\frac{\delta E}{E} \approx \frac{(D_s + D_l)R\theta_e}{(D_l - L_m/2)L_m} \tag{3}$$

where D_l is the distance between the LANEX screen and the start of the magnet, L_m is the length of the magnet, R is the radius of curvature in the magnetic field for an electron of energy E, and D_s is the distance between the source and the start of the magnet. For an electron with an energy of $E = 1.5\,\text{GeV}$, $\delta E/E \approx 5\%$.

The caesium-iodide scintillator A 5 cm thick ceasium-iodide (CsI) scintillator was placed, on-axis, 4m downstream of the electron-laser interaction point. The transverse diameter of each scintillation rod is 5mm, implying an angular resolution of the order of 1.25 mrad. The energy deposited on the scintillator, modelled with FLUKA [37] simulations, is almost linear in the range 10-400 MeV and best fitted (R^2=95%) by: $E_{DEP} = 2.08\times10^{-2}E_{INC}+0.68$ with E_{DEP} and E_{INC} the deposited energy and the energy of the incident photon, respectively. Both energies are in MeV. The scintillation light was then imaged onto a 16-bit EMCCD.

Multi-particle simulations: a beam of 10^7 electrons was generated by sampling from the experimental electron beam spectrum and energy-dependent divergence. First, the electron energy was sampled from the experimental electron spectrum. Second, for each orthogonal axis in the plane perpendicular to the propagation direction the divergence angle was independently sampled from a Gaussian distribution with mean zero and with FWHM given by the experimental electron energy-divergence function calculated at the previously sampled electron energy. Details on the measured energy-dependent divergence are given in the "Laser-wakefield accelerated electron beam" section. Third, the electron three dimensional momentum was calculated from the sampled electron energy and from the two sampled divergence angles. In order to account for the free electron propagation from the gas-cell, the initial transverse electron spatial distribution was obtained assuming ballistic propagation of the electrons over 1 cm from a point-like source.

The longitudinal electron distribution was assumed to be Gaussian with $12\,\mu\text{m}$ FWHM, i.e. $40\,\text{fs}$ duration. The transverse laser pulse field profile was obtained by fitting the experimental transverse profile (see Fig. 1b) with the linear superposition of two Gaussian pulses. Each Gaussian pulse was accurately modelled by including terms up to the fifth order in the

diffraction angle. The resulting peak amplitude of the laser field at the focus was $a_0 \approx 22.5$ with approximately $2.5\,\mu m$ FWHM of the transverse intensity profile. The laser pulse temporal profile was Gaussian with $42\,fs$ duration FMHM of the laser pulse intensity. Since the accelerated electrons lag behind the laser pulse, the head-on collision between the peak of the scattering laser and the peak of the electron beam was set to occur $64\,fs$ after the scattering laser pulse reached the focus. This results in both a reduction of the maximal laser field at the interaction from $a_0 \approx 22.5$ to $a_0 \approx 10$, and into an increased diameter (FWHM of the intensity) from $2.5\,\mu m$ to about $6.9\,\mu m$.

In order to account for shot-to-shot fluctuations of both lasers, simulations were performed with different initial electron spectra corresponding to a band within one standard deviation centred around the average spectrum. In addition, the amplitude of the scattering laser was also varied within a range of $\pm 5\%$, to account for the experimental uncertainty in the measured intensity. The theoretical uncertainty bands corresponding to the above-mentioned simulations are reported in Fig. 4a-d together with the experimental spectra. Four different sets of simulations were performed. In the first set of simulations electrons were evolved with the Lorentz force, and the corresponding Larmor emission energy was calculated during the evolution. In this perturbative approach, similarly to the one adopted in synchrotron machines, the total emitted energy was subtracted after the end of the laser-electron interaction (see Fig. 4a). In the second set of simulations electrons were evolved according to the reduced Landau-Lifshitz equation, i.e. the Landau-Lifshitz equation [1] where the small term containing the derivatives of the electromagnetic field is neglected [38] (see Fig. 4b). Note that, in addition to being negligibly small, the net effect of the terms containing the derivatives of the field average out at zero for a plane-wave pulse [27]. In the third set of simulations, a semiclassical model was employed, where energy losses are still modelled following the Landau-Lifshitz equation but with a correction function $g(\chi)$ multiplying the radiation reaction force, which takes into account that the classical theory overestimates the energy losses compared to the full QED theory. In fact, $g(\chi) = I_Q/I_C$, where:

$$I_Q = \frac{e^2 m_e^2}{3\sqrt{3}\pi\hbar^2} \int_0^\infty \frac{u(4u^2 + 5u + 4)}{(1+u)^4} K_{2/3}\left(\frac{2u}{3\chi}\right) du \tag{4}$$

is the quantum radiation intensity, while $I_C = 2e^2 m_e^2 \chi^2/3\hbar^2$ it the classical radiation intensity (see Eqs. (4.50) and (4.52) in Ref. [39]). In our simulations the following interpolation

formula is employed:

$$g(\chi) \approx \frac{1}{[1 + 4.8(1 + \chi)\ln(1 + 1.7\chi) + 2.44\chi^2]^{2/3}} \tag{5}$$

which approximates the function $g(\chi)$ with accuracy better than 2% for arbitrary χ (see Eqs. (4.57) in Ref. [39]). In the fourth set of simulations a QED approach was employed, where stochastic photon emission was calculated for arbitrary electron and photon energies, and electrons were propagated according to the Lorentz equation between two consecutive photon emission events [40] (see Fig. 4d). As a final remark, we note that the specific polarisation direction of the laser is not relevant for the phenomena under study, as confirmed by our simulations using different polarisation axes.

Particle-In-Cell simulations: Particle-in-cell (PIC) simulations were performed using the code EPOCH [31]. EPOCH uses the same model for radiation reaction as the QED model in the multi-particle simulations described above [41]. EPOCH also includes collective effects due to the charge and current in the electron beam; although the code assumes a charge neutralising background at the initial position of the electron beam in the simulation (thus overestimating the importance of collective effects in the case simulated here). Three dimensional EPOCH simulations were performed. The laser and electron bunch simulated were the same as in the multiparticle simulations. The spatial domain extended over $78.7\,\mu\mathrm{m}$ in the direction of laser propagation (discretised over 1020 cells) and $40\,\mu\mathrm{m}$ in each of the transverse directions (discretised over 920 cells). The collision between the laser pulse and electron bunch occurred 64 fs after the laser pulse reached focus. The electron bunch was represented by 1.5×10^7 macro-particles using third-order particle weighting. The data required to reproduce the PIC simulation results is available in Ref. [42].
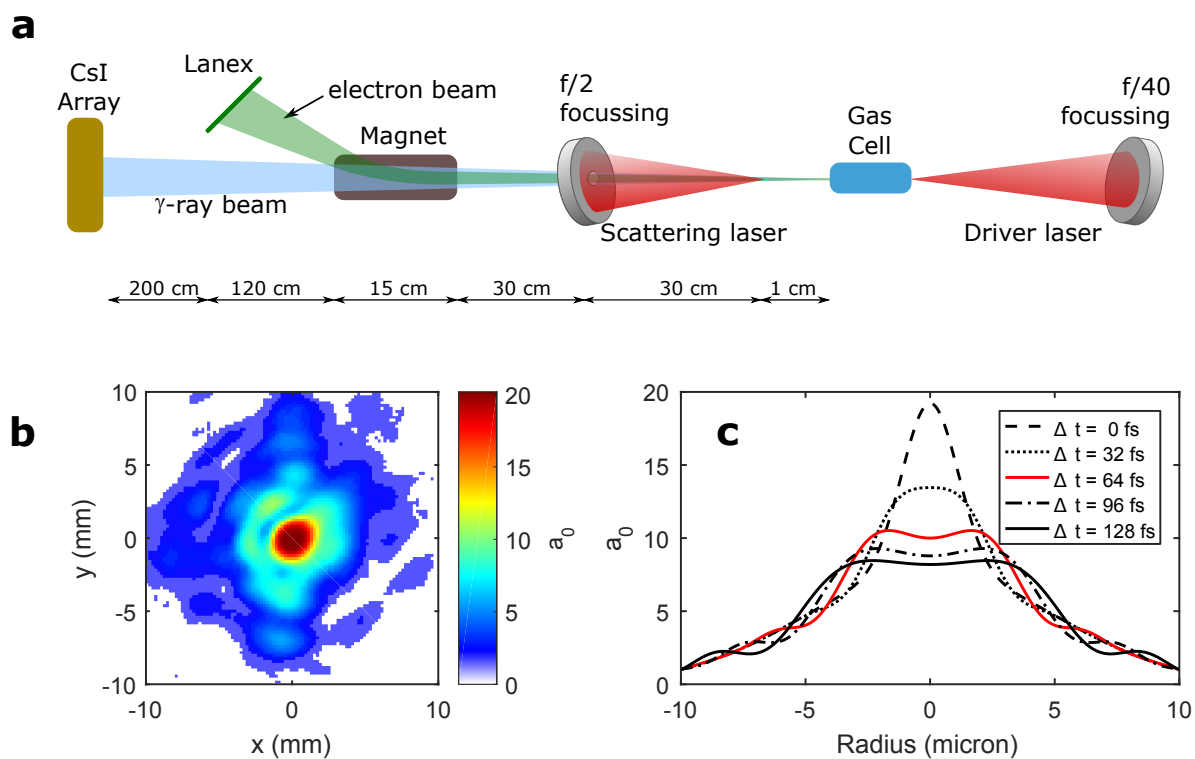
Figure 1. **Experimental setup: a.** Schematic of the experimental setup: details in the text. **b.** Typical measured spatial distribution of the intensity in focus of the <u>Scattering Laser</u> beam. **c.** Computed transverse distribution of the normalised laser field amplitude of the <u>Scattering laser</u> at the overlap point as a function of time. Details in the Methods section.
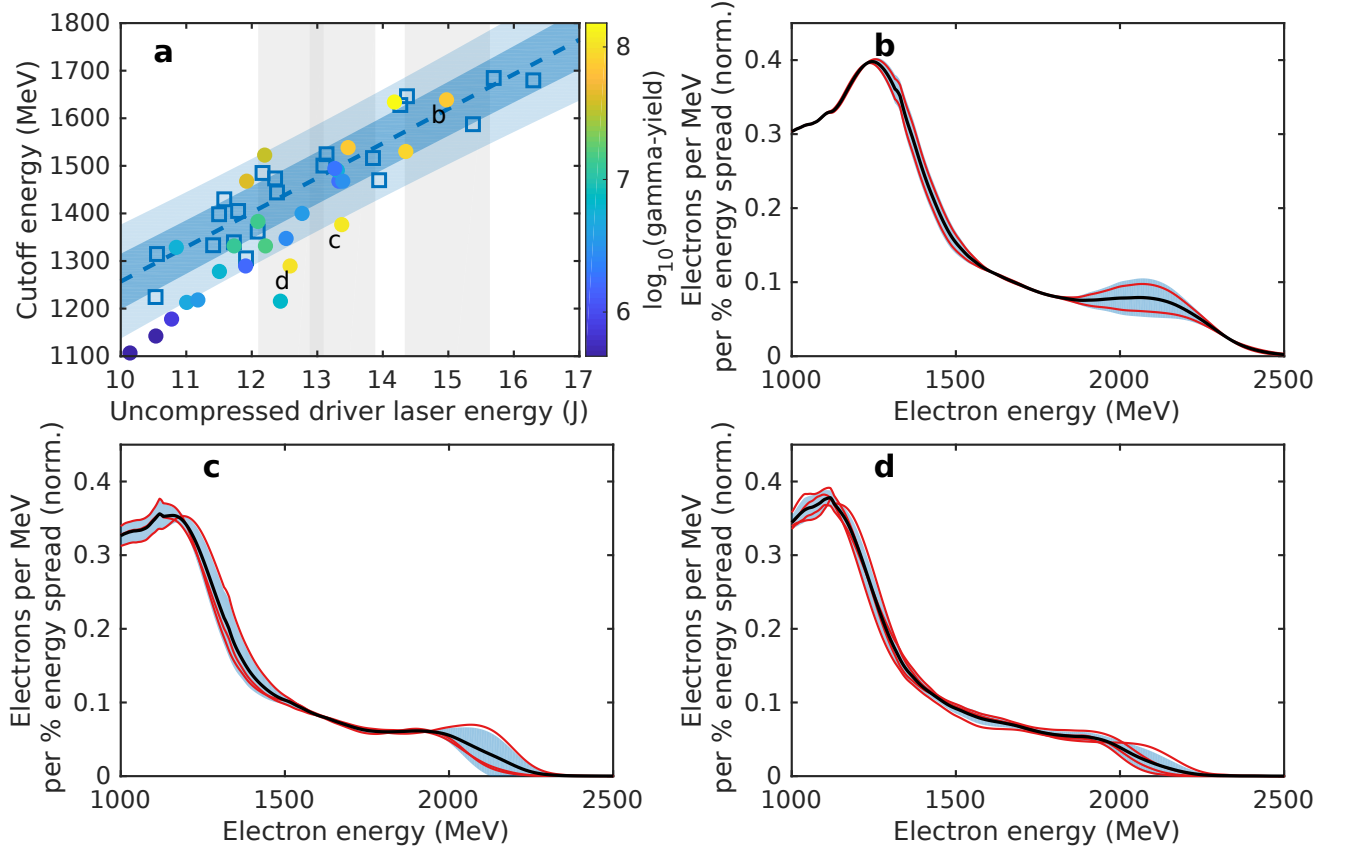
Figure 2. **Reference Electron Spectra: a.** Cut-off energy of the electron beam (defined as the energy at which the number of electrons per MeV drops to 10% of the highest value at low energy) for shots with the Scattering laser off (reference shots, empty squares) and on (colour-coded circles). The dashed blue line represents a linear fit ($R^2 = 0.85$) for the reference shots with the lighter and darker blue bands representing regions of 95% and 68% confidence respectively. The circles are coloured according to the recorded total energy of the emitted photon beam (colorbar on the right, arbitrary units). The shots analysed in the manuscript showing strong (d), weak (c) and negligible (b) radiation reaction are also labelled. The grey bands represents regions from where the reference shots for each of the analysed shots have been selected. **b.** Initial electron spectra (Scattering laser off) for a laser energy between 14.2 and 15.7 J. **c.** Initial electron spectra (Scattering laser off) for a laser energy between 12.9 and 13.9 J. **d.** Initial electron spectra (Scattering laser off) for a laser energy between 12.1 and 13.1 J. In frames b.-d., thin red lines represent single shots, thick black lines represent an average, and the associated bands represent one standard deviation.
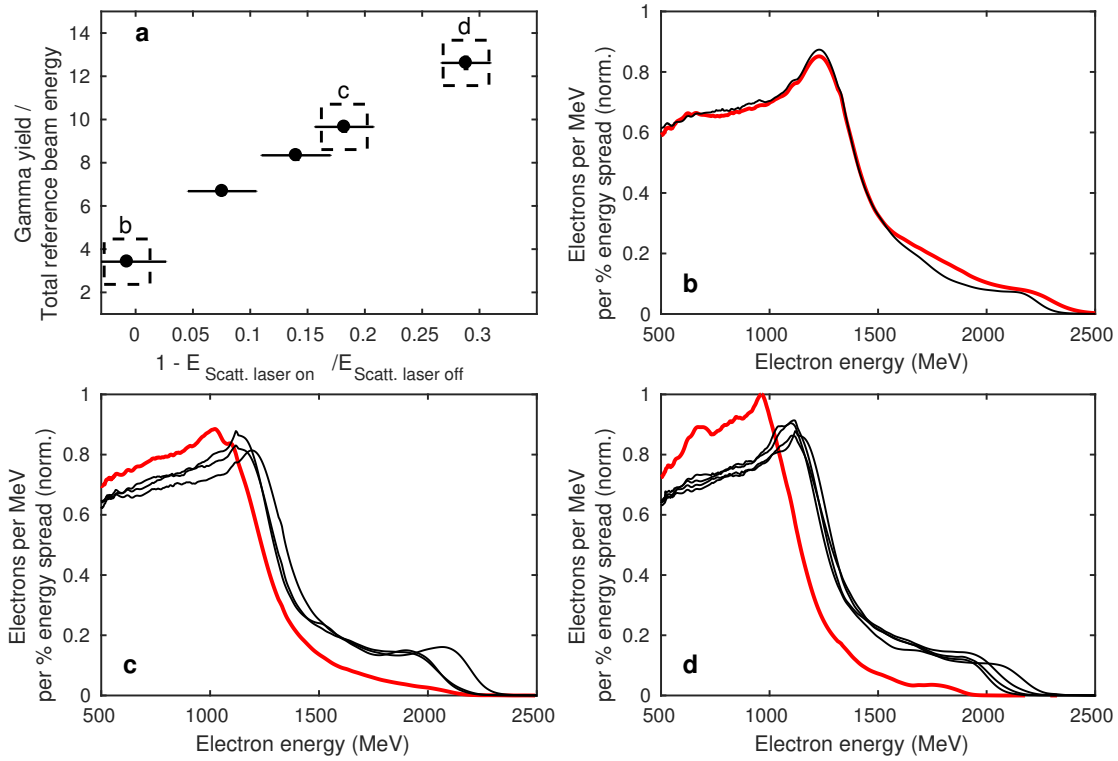
Figure 3. **Radiation Reaction Data: a.** Measured integrated γ-beam photon energy (normalised to the total kinetic energy in the un-scattered electron beam) versus amount of radiation friction experienced by the electron beam. Total friction is estimated by dividing the total kinetic energy in the scattered electron beam by the total kinetic energy in the related reference shot. **b. - d.** Measured electron spectrum after interaction with the scattering laser (thick red line) and related spectra with the scattering laser off (black thin line) for the three different scenarios shown in frame a.: poor overlap (frame b.), moderate overlap (frame c.), and best overlap (frame d.)
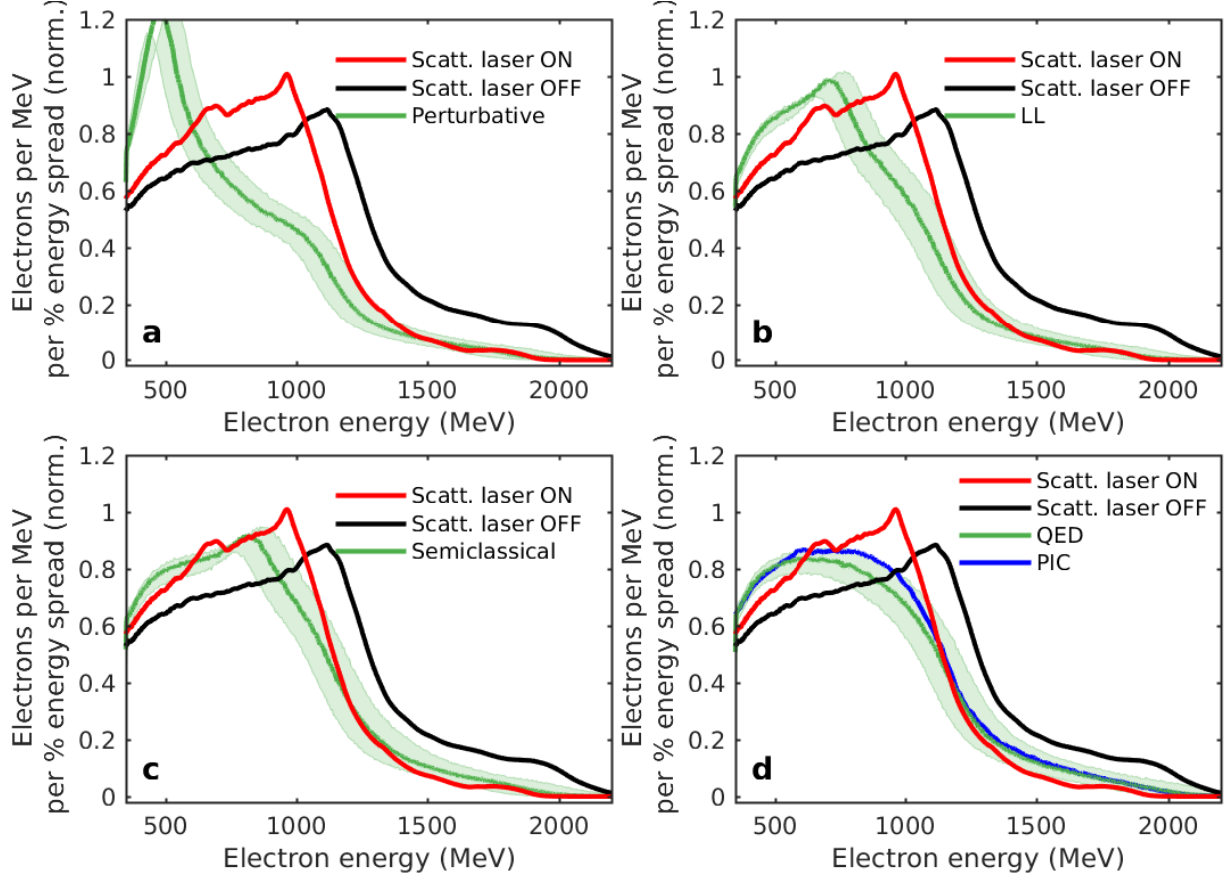
Figure 4. **Comparison of experimental results with theoretical models for the condition of best overlap:** The experimentally measured electron spectrum without the scattering laser (black line) and the spectrum of scattered electrons (red line) and **a.** the theoretical prediction assuming a model only based on the Lorentz force, **b.** the Landau-Lifshitz equation, **c.** a semiclassical model of radiation reaction and **d.** the quantum model of radiation reaction in a multi-particle code and in a PIC code (green and blue curves, respectively). In each frame, the uncertainties associated with the theoretical model arise from assuming the experimental uncertainty in the original electron spectrum, as arising from the energy uncertainty of the magnetic spectrometer, and shot-to-shot intensity fluctuations of the scattering laser. Details of the models used are discussed in the Methods section.